MnCuFe/P-GCE Electrochemical Sensor: A Breakthrough Catalyst for Highly Sensitive Detection of Methyl Parathion in Diverse Matrices

Sharmila Tharuman[a], Nandini Nataraj[a], Shen-Ming Chen [a,*]

[a]*Department of Chemical Engineering and Biotechnology, National Taipei University of Technology, No.1, Section 3, Chung-Hsiao East Road, Taipei 106, Taiwan.*

***Corresponding author**: smchen@ntut.edu.tw (S.M. Chen)

S1. Materials and Reagents

Manganese nitrate tetrahydrate ($Mn(NO_3)_2.4H_2O$), copper nitrate trihydrate ($Cu(NO_3)_2.3H_2O$), trisodium citrate ($Na_3C_6H_5O_7$), sodium hypophosphite monohydrate ($NaH_2PO_2{\cdot}H_2O$), sodium phosphate monobasic dihydrate ($H_2NaO_4P.2H_2O$), sodium phosphate dibasic (HNa_2O_4P), potassium chloride (KCl), potassium ferricyanide ($K_3Fe(CN)_6$), potassium ferrocyanide ($K_4Fe(CN)_6.3H_2O$), lead acetate trihydrate ($Pb(C_2H_3O_2)_{2.3}(H_2O)$), chromium chloride hexahydrate ($CrCl_3.6H_2O$), iron nitrate nonahydrate ($Fe(NO_3)_3.9H_2O$), ascorbic acid, D-glucose, mesalamine, nilutamide, and uric acid were purchased from sigma-aldrich and used without further purification.

S2. Characterization

A variety of analytical methods were employed to characterize the prepared sample comprehensively. The structural and crystalline properties of the sample were assessed using X-ray diffraction with a PANalytical XPert PRO X-ray diffractometer, which utilized Cu-Kα radiation (λ=0.1541 nm) to identify the material's crystal structure and crystallinity. Fourier transform infrared spectroscopy (FT-IR), specifically using Jasco's V-6600 instrument, was used to determine the functional groups present in the sample, providing insights into its chemical bonds and functional groups. The optical properties of the prepared materials were investigates using UV–vis NIR spectrometer (JASCO V-750). Photoluminescence (PL) for samples were recorded using Perkin Elmer fluorescence spectrometer L2250106-LS 45, to analyze the charge separation ability of obtained nanocomposite. To investigate the chemical states of the elements within the sample, X-ray photoelectron spectroscopy (XPS) was employed, with analysis conducted using the ESCALAB 250 system from Thermo Scientific Ltd in the Netherlands. The chemical interactions and molecular characteristics of the sample

were explored using Raman spectroscopy with the Raman Dong Woo 500 I instrument from Korea. The sample's morphological features and elemental composition were thoroughly examined using advanced microscopy techniques, including Field Emission Scanning Electron Microscope (FESEM) and Transmission Electron Microscope (TEM). FESEM provided high-resolution images for detailed observations of the sample's surface morphology, while a Philips CM 200 transmission electron microscope was used to investigate the internal structure and finer details of the sample at the nanoscale level. Energy-Dispersive X-ray Spectroscopy (EDX) analysis, in conjunction with FESEM, was employed to precisely determine the sample's elemental composition and gain insights into the distribution of elements within the material.

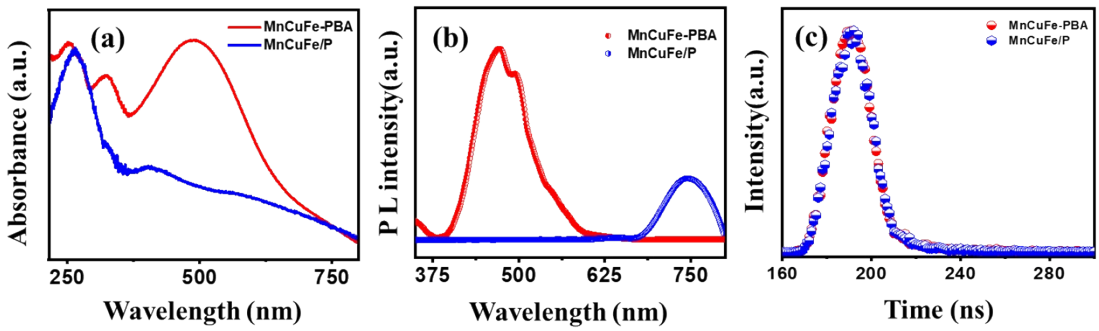

Figure S1. MnCuFe-PBA and MnCuFe/P's (a) UV-DRS spectra, (b) PL-spectra and (c) TRPL spectra.

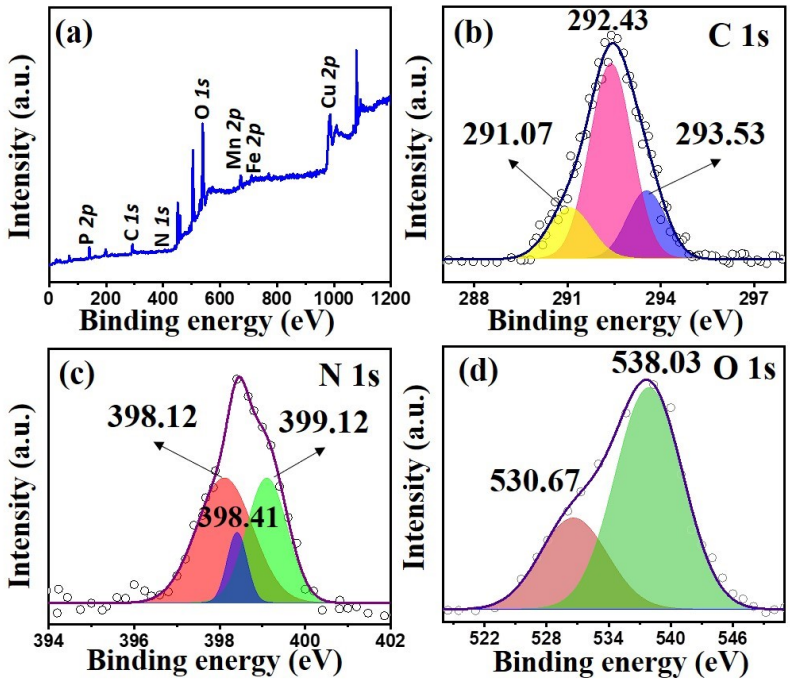

Figure S2. XPS analysis of MnCuFe/P **(a)** full survey, **(b)** C 1s, **(c)** N 1s, and **(d)** O 1s.

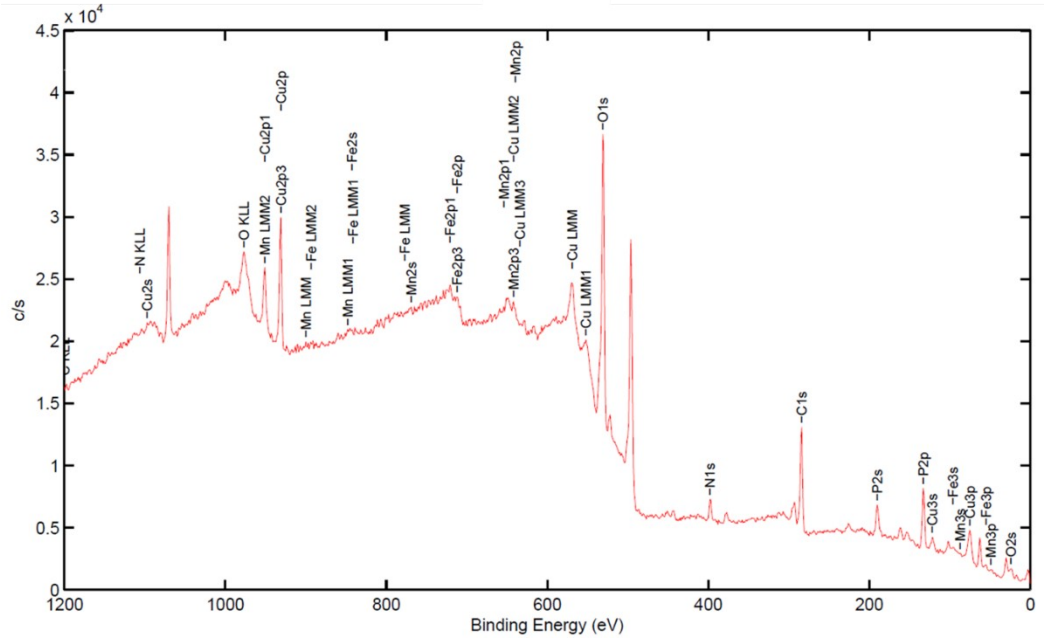

Figure S3. Cu LLM spectra of MnCuFe/P.

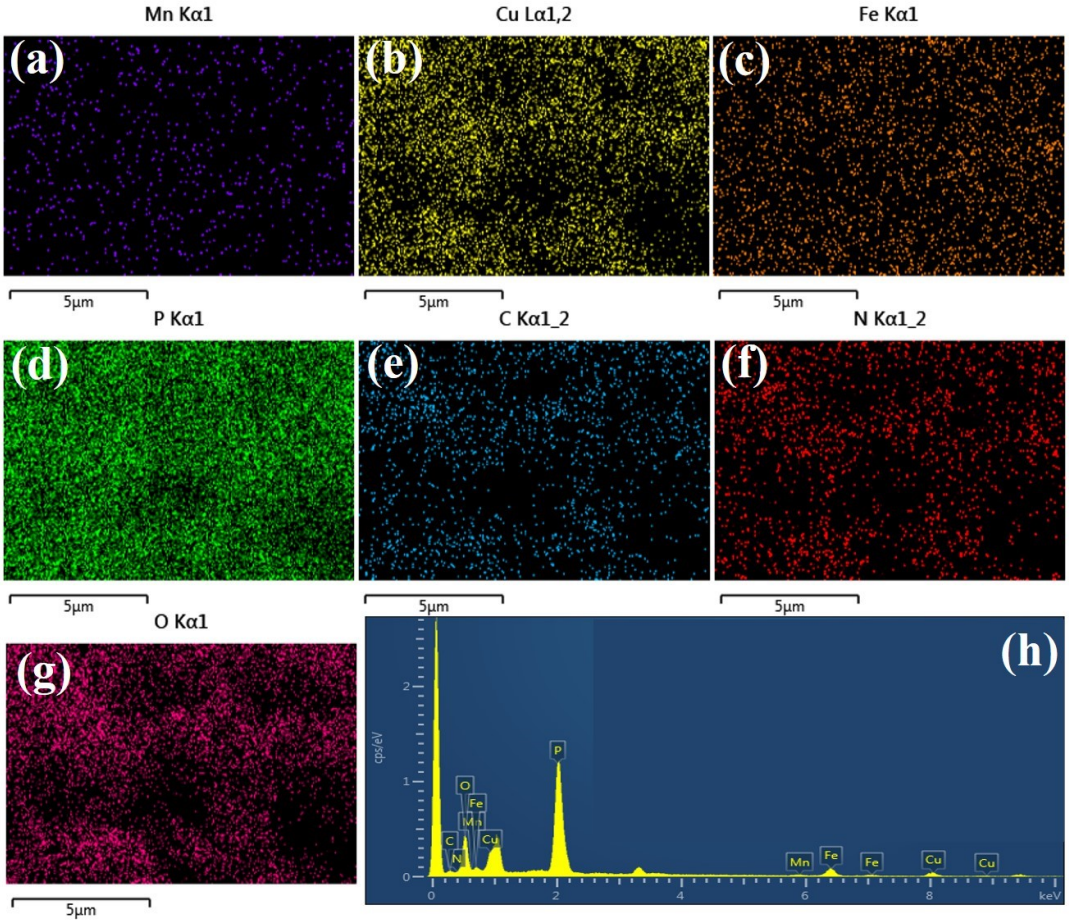

Figure S4. Elemental mapping of MnCuFe/P (a–g) EDX spectrum of MnCuFe/P (h).

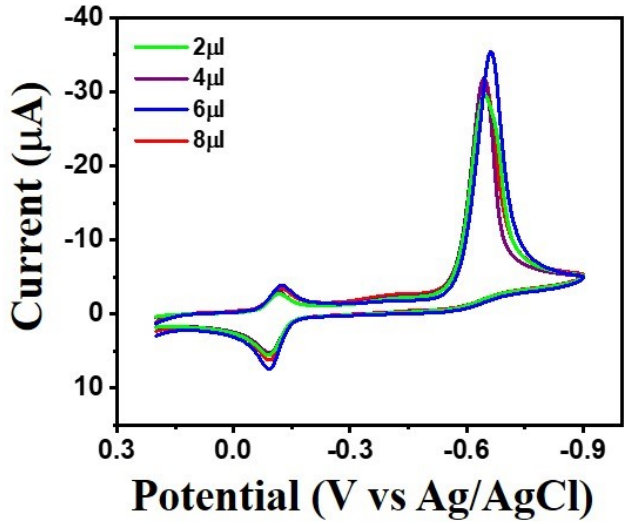

Figure S5. CV studies at pH-7 for MnCuFe/P-GCE at a scan rate of 50 mV/s with 150 µM MP addition for microliter optimisation.

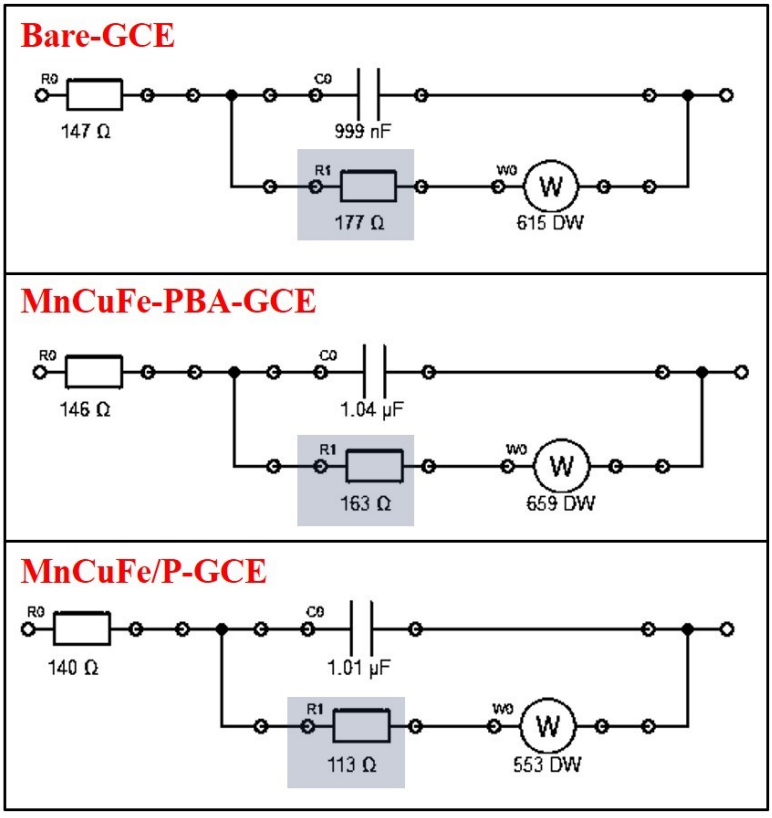

Figure S6. Randles circuit fitted using Zanher analysis software here R_0 is R_s, R_1 is R_{ct}, C_0 is C_{dl} and W_0 is Z_w.

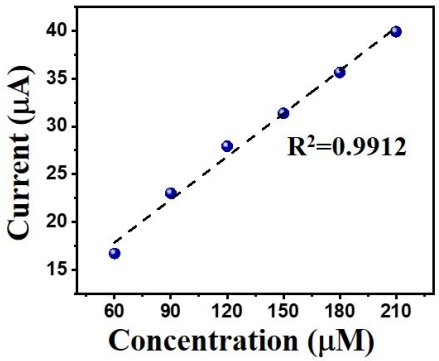

Figure S7. The linear regression between the concentration and current at pH-7 for MnCuFe/P-GCE at a scan rate of 50 mV/s for different MP concentration.

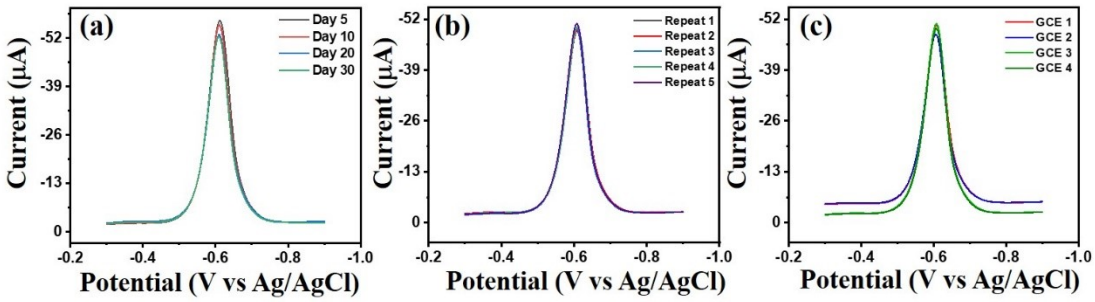

Figure S8. DPV curves obtained for MnCuFe/P-GCE with 150 μM MP at pH-7 **(a)** stability **(b)** repeatability and **(c)** reproducibility.

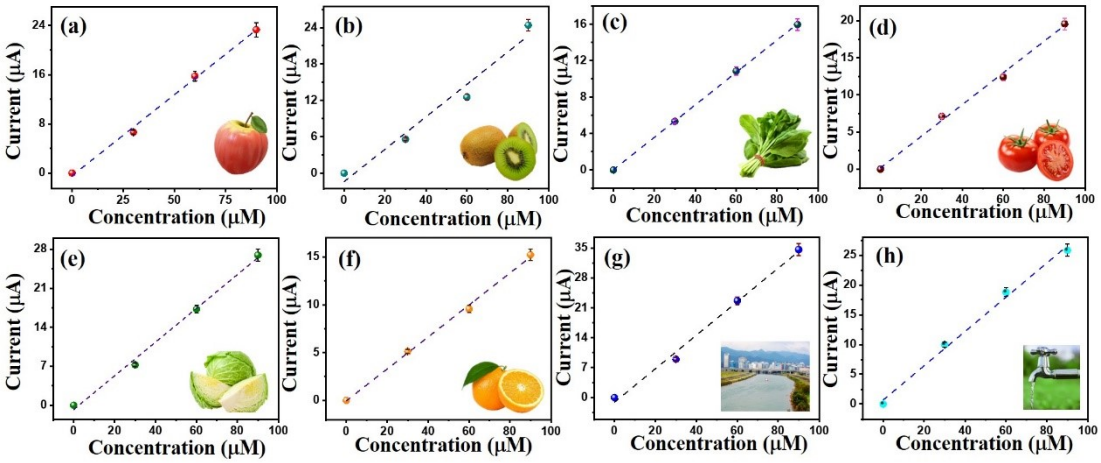

Figure S9. Calibration plot for the CV curves obtained for real samples done at MnCuFe/P-GCE in **(a)** apple, **(b)** kiwi, **(c)** spinach, **(d)** tomato, **(e)** cabbage, **(f)** orange, **(g)** river water, and **(h)** tap water.

Table S1. Electrochemical detection of MP in various real samples

Real sample	**Added (μM)**	**Found (μM)**	**Recovery (%)**
Apple	0	0	0
	30	26.79	89.33
	60	61.46	102.5
	90	90.07	100.1
Kiwi	0	0	0
	30	26.15	87.15
	60	52.12	86.87
	90	96.51	107.24
Spinach	0	0	0
	30	30.17	100.55
	60	61.24	102.07
	90	89.83	99.82
Tomato	0	0	0
	30	34.2	114
	60	58.99	98.32
	90	92.58	102.86
Cabbage	0	0	0
	30	21.43	71.43
	60	54.48	90.79

	90	86.46	96.07
Orange	0	0	0
	30	30.89	102.96
	60	57.51	95.85
	90	91.38	101.53
River water	0	0	0
	30	25.63	85.42
	60	60.59	100.98
	90	91.08	101.19
Tap water	0	0	0
	30	32.26	107.54
	60	62.87	104.78
	90	87.34	97.04